

High-resolution x-ray-photoemission study of metastable Fe silicide core-electron states

S. Hong, U. Kafader,* P. Wetzel, G. Gewinner, and C. Pirri

*Laboratoire de Physique et de Spectroscopie Electronique, Faculté des Sciences et Techniques 4 rue des Frères Lumière,
68093 Mulhouse Cédex, France*

(Received 31 October 1994; revised manuscript received 21 March 1995)

The core-electron states of metastable pseudomorphic Fe silicides, epitaxially grown on Si(111), have been measured by monochromatized x-ray photoemission. These silicides have been grown by molecular-beam epitaxy with composition ranging from FeSi up to FeSi₂. Si 2*p* and Fe 2*p*_{3/2} core lines have been compared to those measured on both polycrystalline and epitaxially grown stable β-FeSi₂ and ε-FeSi layers. Metastable silicide related Si 2*p* and Fe 2*p*_{3/2} core line binding-energy shifts, with respect to β-FeSi₂ or clean Si(111), have been interpreted as arising from electron charge transfer from Si to Fe, in agreement with recent calculations. Si 2*p* and Fe 2*p*_{3/2} binding energies as well as line-shape evolutions, over a wide composition range, give strong support to a model with a nearly cubic structure, evolving from FeSi to FeSi₂, in which Fe atoms are randomly distributed over the Si cages.

I. INTRODUCTION

A lot of effort has recently been made to produce high-quality Fe silicides epitaxially grown on Si(111). The main goal was to achieve perfect β-FeSi₂ layers. β-FeSi₂ could be used as a constituent of Si-based optoelectronic devices (semiconductor-based heterojunctions) since it has a band gap of ~0.85 eV.¹ Epitaxy of β-FeSi₂ has been approached by numerous experimental ways, including solid phase epitaxy (SPE), molecular-beam epitaxy (MBE), metal-organic chemical-vapor deposition (MOCVD), and ion implantation. It has been shown that, during the growth process of β-FeSi₂, stable as well as metastable Fe silicides can be epitaxially grown on Si(111). Furthermore, in some cases the microstructure and epitaxial orientations can be strongly influenced by the metastable silicide phases formed during the growth process.^{2,3} In particular, β-FeSi₂ layer quality (domain size, single orientation, etc.) is improved upon rapid thermal annealing of SPE-grown β-FeSi₂ layers.³ With this procedure, β-FeSi₂ transforms into a metastable metallic cubic phase and back to the semiconducting β-FeSi₂ phase.

The crystallographic structure of both stable and metastable phases has been extensively studied.²⁻¹⁴ Silicides with very different structures can be grown on Si(111) with their own electronic properties. In its stable phase, FeSi crystallizes in a B-20 structure and is a narrow-gap semiconductor (0.05 eV),^{15,16} while in its metastable form, it crystallizes in a CsCl-type structure and is metallic.⁷ This latter phase persists typically up to 300°C (this temperature depends on the film thickness). FeSi₂ has two stable forms. Below 950°C, it crystallizes in the orthorhombic structure, the semiconducting β-FeSi₂, and above this temperature it crystallizes in the tetragonal α-FeSi₂ structure and is metallic.¹⁷ A tetragonal FeSi₂ phase can be stabilized at room temperature by SPE or MOCVD on Si(111) giving rise to an α-FeSi₂ derived structure.¹² Alternatively, a cubic CsCl-type FeSi₂ phase

has been synthesized by molecular-beam epitaxy on Si(111).⁴ These disilicides are typically stable up to 500°C. Most interestingly, Fe silicides with variable stoichiometry, from pure Fe up to FeSi₂, can be epitaxially grown on Si(111), even at room temperature.^{2,7,14}

Numerous theoretical and experimental investigations of the electronic structure of both stable and epitaxy induced Fe silicide phases have been performed.¹⁷⁻³¹ Among these studies, the core-electron states of the stable bulk phases have recently been investigated by means of high-resolution photoemission experiments using synchrotron radiation.³⁰ However, no experimental information about the pseudomorphic metastable silicide core-electron states has been available up to now, to our knowledge.

In this paper we report on Si 2*p* and Fe 2*p*_{3/2} core-level measurements by means of monochromatized x-ray photoemission. The core-level lines were measured on epitaxial pseudomorphic Fe silicides, with stoichiometries ranging from FeSi to FeSi₂. They were grown on Si(111) 7×7 by codeposition of Fe and Si at room temperature. The core-level evolution versus temperature is also investigated and all data are compared to those measured on epitaxial and polycrystalline stable ε-FeSi and β-FeSi₂ phases.

II. EXPERIMENT

The experiments have been performed in an ultrahigh vacuum system with base pressure below 8×10⁻¹¹ mbar. It was equipped with a Leybold Heraeus EA 200 electron spectrometer for angle-resolved ultraviolet photoemission spectroscopy, x-ray photoemission spectroscopy, and with a low-energy electron diffraction (LEED) optics. The photoemission spectra were recorded with both monochromatized and unmonochromatized Al Kα sources (ħω=1486.6 eV). The photoelectrons were analyzed using a hemispherical energy analyzer (150 mm in radius) with 50-meV energy resolution and an 18 channels multidetection assembly. The acceptance angle of

the analyzer was set to $\pm 8^\circ$. The overall energetic resolution using the monochromatized Al $K\alpha$ source was about 0.5 eV.

The pseudomorphic FeSi_x ($1 < x < 2$) silicides were prepared by codeposition of Fe and Si onto substrates held at room temperature (RT). The Si(111) substrates were cleaned by a thermal annealing above 800°C . After sample introduction in the UHV system, its temperature is increased very slowly (a few hours) up to 850°C . This procedure results in a well-ordered contaminants free (carbon and oxygen) Si(111) surface. Its crystallinity was attested by a sharp 7×7 LEED pattern. Fe and Si were evaporated from boron nitride and carbon crucibles, respectively, at stable and reproducible rates in the 1–2 $\text{\AA}/\text{min}$ range. These low evaporation rates, checked independently for Si and Fe using quartz-crystal microbalances, allowed the fabrication of silicides with well-controlled stoichiometry. First, a thin (6–9 \AA) FeSi_2 layers was co-deposited onto the Si(111) substrate and was annealed at 500°C resulting in an epitaxial FeSi_2 template layer characterized by a sharp 2×2 LEED pattern. Second, 90- \AA -thick epitaxial Fe silicide layers were codeposited onto this template. These silicides have been annealed in the RT– 600°C temperature range and their crystallinity was checked using LEED optics. Their composition was also controlled by measuring the Fe $2p_{3/2}$ to Si $2p$ core-level area ratio, which is compared to those measured on the stable $\beta\text{-FeSi}_2$ one. These core levels were recorded at normal emergence with the unmonochromatized Al $K\alpha$ source.

III. RESULTS

Metastable as well as stable silicide crystallinity has been followed by LEED. For a composition ranging from FeSi to FeSi_x , with x close to 2, room-temperature-deposited silicides are epitaxial as attested by 1×1 LEED patterns with a well-marked threefold symmetry. As pointed out previously,¹⁴ the LEED pattern quality (spot sharpness, diffuse background intensity, etc.) depends on the silicide stoichiometry. The spot-to-background intensity ratio was found to decrease as a function of Si content from $\text{FeSi}_{1.5}$ to FeSi_2 . For depositions in a ratio close to FeSi_2 , some silicide layers are epitaxial and exhibit a 1×1 LEED pattern, while for others one observes only a strong diffuse background. Yet, the ordered-to-disordered transition is not as sharp as the LEED experiments would indicate. Inelastic medium-energy-electron diffraction (IMEED) patterns observed at electron energies of about 1000 eV indicate a progressive evolution from ordered (1×1 LEED pattern) -to-disordered (neither LEED nor IMEED diagram) layer, through a situation in which the LEED pattern is washed out but the IMEED diagram is still visible. In this latter case the silicide layers are textured but the long-range-order coherence necessary for LEED observations is no longer preserved. IMEED diagrams arise from inelastic back-scattered electrons and exhibit angular distributions very similar to that of Auger electrons or x-ray photoelectrons.³² It provides similar structural information on local atomic structure and epitaxial orientation. The

LEED and IMEED diagrams obliteration occurs at a stoichiometry very close to the FeSi_2 , as evidenced by Fe $2p_{3/2}$ to Si $2p$ core-level area ratio measurements, shown in Table I along with that of $\beta\text{-FeSi}_2$.

In any case, the LEED pattern quality is improved by annealing. Silicides with composition close to FeSi_2 also exhibit a 1×1 LEED pattern, whatever the RT LEED pattern is. The temperature range in which these layers can be annealed is, however, limited. Indeed, these codeposited FeSi_x silicides undergo metastable-to-stable transitions upon annealing.^{7,14,25} The transition temperature depends on several parameters such as stoichiometry, film thickness, or growth methods. Typically, at a given film thickness (90 \AA), the metastable-to-stable phase-transition temperature increases as a function of Si content.

The 90- \AA -thick pseudomorphic FeSi phase is stable up to $\approx 300^\circ\text{C}$ in agreement with previous findings⁷ and it exhibits a 1×1 LEED pattern. It transforms into $\epsilon\text{-FeSi}$ at $350\text{--}400^\circ\text{C}$ and into $\beta\text{-FeSi}_2$ above 550°C . For such thick films, both $\epsilon\text{-FeSi}$ and $\beta\text{-FeSi}_2$ are polycrystalline.²⁵ The FeSi_2 transition towards the stable $\beta\text{-FeSi}_2$ occurs at about 550°C . Upon annealing codeposited FeSi_x ($x \sim 2$) layers at $\sim 400\text{--}450^\circ\text{C}$ the LEED pattern is 2×2 . For thinner pseudomorphic FeSi_2 silicides (with thickness typically below 15–20 \AA) the transition occurs at higher temperature since these metastable phases are stabilized by epitaxy.² Thin codeposited as well as SPE-grown FeSi_2 layers, annealed at $500\text{--}550^\circ\text{C}$ exhibit a sharp 2×2 LEED superstructure. The relevant surface was found to be Si terminated by ion-scattering spectroscopy and scanning tunneling spectroscopy.³³ Ordered Si adatoms on top of the silicide are mainly responsible for the 2×2 reconstruction. A similar reconstruction could be at the origin of the 2×2 LEED pattern observed for the 90- \AA -thick Si-rich silicides considered in this work. At any composition, the Fe $2p_{3/2}$ to Si $2p$ area ratio was measured before and after annealing. No significant decrease of this ratio was observed, showing that there is no additional Si diffusion from the substrate. The silicide composition is not affected by annealing at temperature indi-

TABLE I. Fe $2p_{3/2}$ to Si $2p$ core-line area ratio for room-temperature-deposited metastable Fe silicides and 600°C annealed $\beta\text{-FeSi}_2$. Core lines were collected at normal electron emergence with an unmonochromatized Al $K\alpha$ source ($\hbar\omega = 1486.6$ eV). The metastable silicide composition is inferred from Si and Fe codeposition rates during the growth at room temperature.

Compounds	LEED pattern (room temperature)	Fe $2p_{3/2}$ /Si $2p$ area ratio (room temperature)
$\beta\text{-FeSi}_2$	no	3.9
FeSi	1×1	9.1
$\text{FeSi}_{1.3}$	1×1	7.9
$\text{FeSi}_{1.5}$	1×1	6.4
$\text{FeSi}_{1.8}$	1×1	5.5
FeSi_2	1×1	4.5
FeSi_2	no	4.1

cated previously. This ratio is slightly increased upon annealing Si-rich silicide reflecting an improvement of the crystallinity. Both Fe $2p_{3/2}$ and Si $2p$ line areas are enhanced by forward focusing effects. This increase is of $\sim 11\%$ for the Fe $2p_{3/2}$ line and $\sim 6\%$ for the Si $2p$ line.

The stable ϵ -FeSi (β -FeSi₂) phase can be obtained either by SPE or by annealing at 400°C (650°C) MBE-grown FeSi (FeSi₂) pseudomorphic layers. Depending on the silicide thickness, epitaxial or polycrystalline β -FeSi₂ and ϵ -FeSi grow on Si(111). For thicknesses typically below 15–20 Å, epitaxial ϵ -FeSi and β -FeSi₂ layers are achieved. They are characterized by specific LEED patterns. ϵ -FeSi crystallizes in a simple cubic structure ($B20$) with a lattice parameter $a = 4.483$ Å. Epitaxial ϵ -FeSi grows with (111) ϵ -FeSi|| (111) Si and [011] ϵ -FeSi|| [211] Si.³⁴ The lattice mismatch is about -4.7% and the relevant LEED pattern is $\sqrt{3} \times \sqrt{3} R 30^\circ$. Upon annealing at 650°C thin FeSi₂ layers, epitaxy of β -FeSi₂ can be achieved and results in a complex LEED pattern with a 12-fold symmetry.³⁵ Such a diagram corresponds to a series of silicide domains rotated relative to each other with the (100) plane parallel to the Si(111) surface.

Figures 1 and 2 show the Si $2p$ lines measured on as-deposited 90-Å-thick metastable Fe silicides and after annealing just below the pseudomorphic-to-stable phase

transition temperature, respectively. These spectra are presented along with that of stable ϵ -FeSi, β -FeSi₂, and clean Si(111). Figure 3 compares the Si $2p$ core lines measured on several RT-grown and annealed metastable silicides. Fe $2p_{3/2}$ lines recorded on both stable and metastable Fe silicides are shown in Fig. 4. The photoemission spectra of Figs. 1–4 were obtained with a monochromatized Al $K\alpha$ radiation and were collected at normal electron emergence. The silicide thicknesses were chosen large enough (90 Å) to avoid substrate contribution to the signal and to minimize surface effects. The ϵ -FeSi and β -FeSi₂ related Si $2p$ lines have been measured on both thick polycrystalline and thin epitaxial layers. No major differences are detected as far as binding energies and line shapes are concerned.

The ϵ -FeSi and β -FeSi₂ Si $2p$ lines are centered at binding energies very close to that of a clean Si(111) surface. The ϵ -FeSi related Si $2p$ line is shifted by about 0.15 eV towards low binding energies, with respect to the Si(111) 7×7 ones, in a fairly good agreement with results of Ref. 30. The β -FeSi₂-related Si $2p$ line shift with respect to the Si(111) ones is very small (< 0.05 eV). Both ϵ -FeSi and

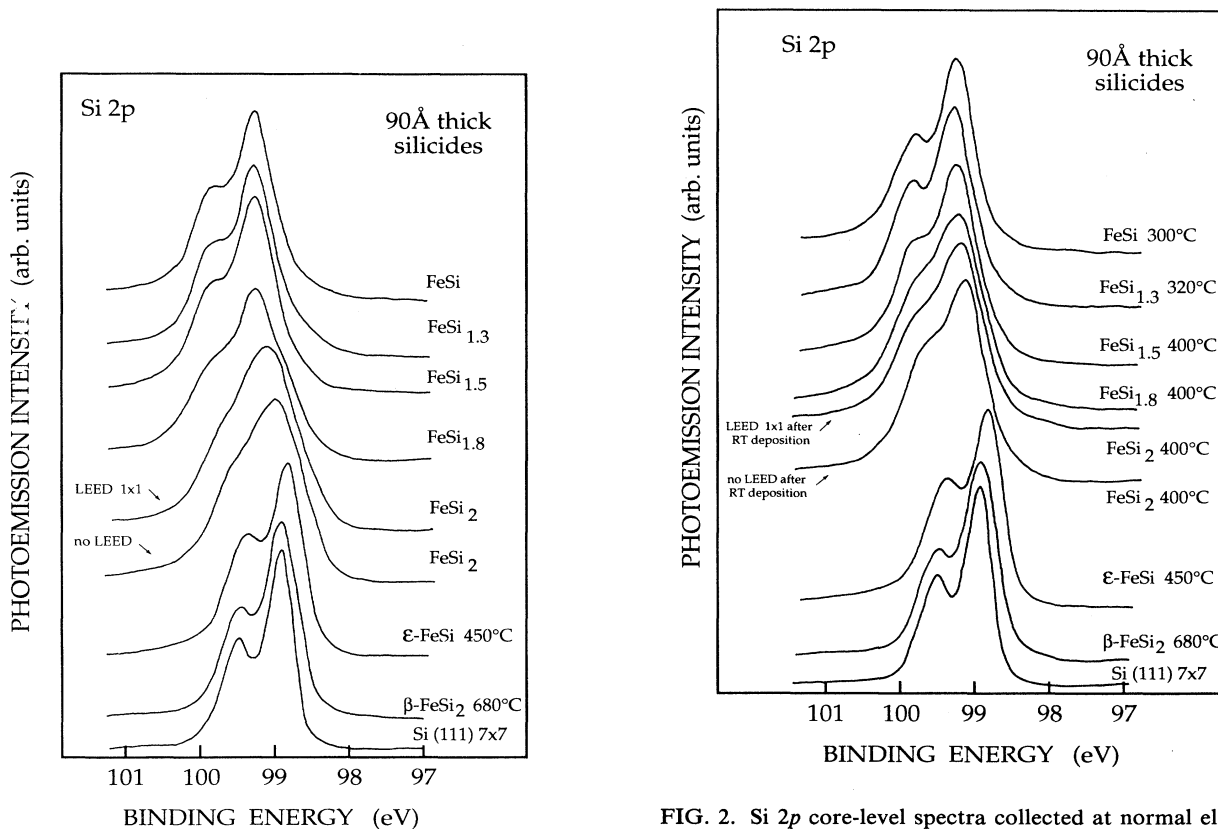


FIG. 1. Si $2p$ core-level spectra collected at normal electron emergence for clean Si(111) surfaces, β -FeSi₂, ϵ -FeSi, and room-temperature codeposited pseudomorphic FeSi_x silicides. Spectra were recorded using a monochromatized Al $K\alpha$ source at a photon energy of 1486.6 eV.

FIG. 2. Si $2p$ core-level spectra collected at normal electron emergence for clean Si(111) surfaces, β -FeSi₂, ϵ -FeSi, and annealed pseudomorphic FeSi_x silicides. Spectra were recorded using a monochromatized Al $K\alpha$ source at a photon energy of 1486.6 eV. The FeSi₂ spectra displayed in this figure are those measured after annealing ordered (1×1 LEED pattern) and disordered (no LEED pattern) RT-deposited FeSi₂ layers.

β -FeSi₂ related spin-orbit-split Si 2p_{1/3} and Si 2p_{3/2} lines are slightly less resolved than for clean Si(111). Their line shape arises from different physical origins. The Si 2p line in ϵ -FeSi is composed of two asymmetric Si 2p_{1/2} and Si 2p_{3/2} lines. This asymmetry is reflected in the apparent branching ratio (Fig. 1) and is also observed for the Fe 3p (Ref. 30) and Fe 2p_{3/2} core lines. The origin of this asymmetry is not clearly established (see below). It seems not to be related to several chemically shifted Si 2p or Fe 2p_{3/2} (Fe 3p) components since in ϵ -FeSi, all Si or Fe atoms have identical atomic environments. In β -FeSi₂, two kinds of nearly tetrahedral Si sites contribute to the Si 2p line. On each site, Si is bounded to four Fe atoms at distances ranging from 2.333 Å to 2.437 Å and six Si atoms at distances ranging from 2.499 Å to 3.562 Å.³⁶ However, for both sites, Si atoms are equally coordinated with quite the same number of nearest and next-nearest neighbors and valence angles. Thus the binding-energy difference is expected to be rather small as indeed observed in Fig. 1.

Figures 1 and 2 show that all metastable silicides Si 2p lines are substantially shifted towards higher binding energies, with respect to clean Si(111) or β -FeSi₂, over a wide composition range. After room-temperature deposition, Si 2p lines are shifted by about 0.35 eV, with respect to clean Si(111) or β -FeSi₂, from FeSi up to FeSi_{1.8} composition. In that case, the main difference between Si 2p

spectra resides in the growth of additional Si 2p components, giving rise to a broad tail at low binding energies. Nevertheless, the Si 2p line intensity maximum remains centered at the same binding energy. Upon annealing at 300–400°C, this tail is partially removed and the spin-orbit-split doublet resolution is improved, as shown in Fig. 2. The FeSi-related core line binding energy does not change upon annealing at 300°C, but the Si 2p line slightly sharpens giving rise to a well-resolved Si 2p_{1/2}-Si 2p_{3/2} doublet. Except the small tail at low binding energies, the Si 2p line is comparable to that of the stable ϵ -FeSi phase and indicates that all Si atoms reside in rather well-defined and equivalent sites. These results agree very well with structural characterization of pseudomorphic FeSi.^{7,14} Indeed x-ray diffraction (XRD) as well as extended x-ray-absorption fine-structure (EXAFS) experiments have shown that FeSi has a regular cubic CsCl-type structure, in which each Fe or Si atom has the same atomic environment. Crystallographic structures of CsCl FeSi and α -FeSi₂ are shown in Fig. 5. α -FeSi₂ crystallizes in a quadratic structure.³⁷

Upon by increasing the Si content in the RT-grown silicides, the intensity of the component(s) lying at low binding energy increases, leading to very similarly shaped broad lines for FeSi_{1.8} and FeSi₂. However when the composition becomes very close to FeSi₂, the Si 2p line shifts towards lower binding energies as compared to

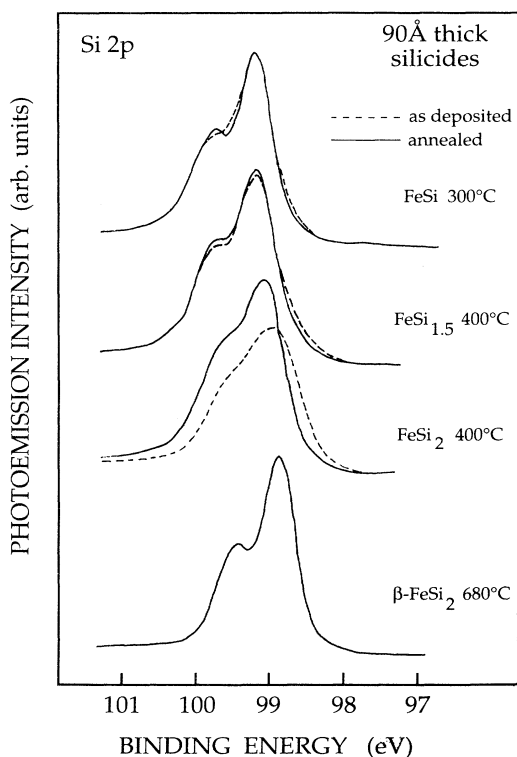


FIG. 3. Comparison of the Si 2p core lines measured on several RT-grown and annealed metastable FeSi_x silicides.

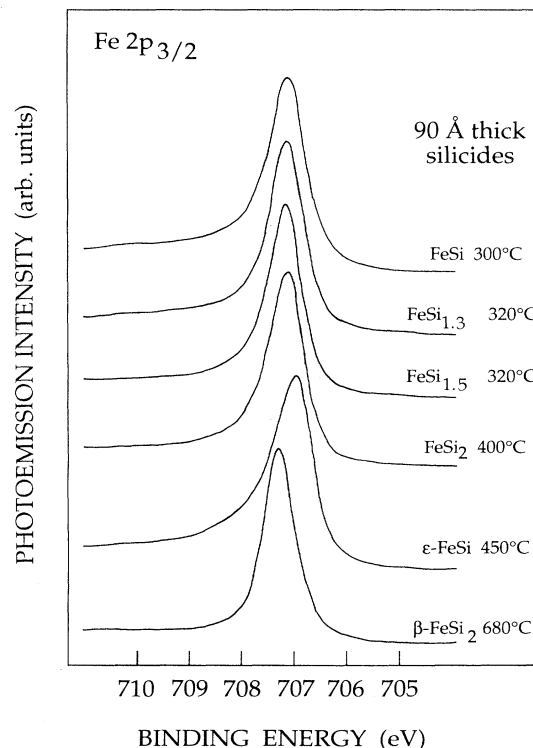


FIG. 4. Fe 2p_{3/2} core-level spectra collected at normal electron emergence for β -FeSi₂, ϵ -FeSi, and pseudomorphic FeSi_x silicides. Spectra were recorded using a monochromatized Al K α source at a photon energy of 1486.6 eV.

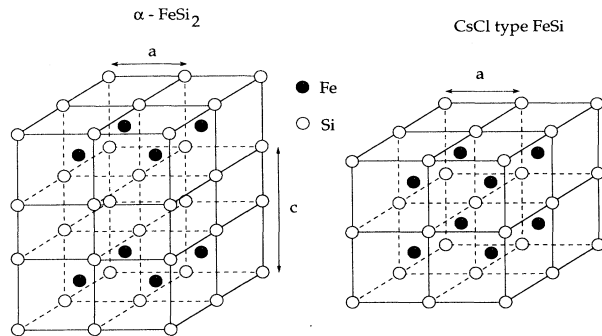


FIG. 5. Structure of CsCl-type FeSi and tetragonal α -FeSi₂.

FeSi or FeSi_{1.8}. It seems that this change in Si 2*p* line position takes place in correlation with the LEED pattern degradation. The Si 2*p* line shift, with respect to clean Si(111) or β -FeSi₂, decreases from 0.2 eV when the 1×1 LEED pattern is still visible, down to a value of ~0.1 eV when the LEED is washed out. This Si 2*p* binding-energy evolution is remarkable since it occurs in a very small (FeSi_{1.8} to FeSi₂) composition range. As previously shown, a 2×2 LEED pattern is recovered upon annealing at 400–450 °C for both ordered (1×1 LEED pattern) and disordered (no LEED) RT-deposited FeSi_{*x*} (*x* ~ 2) silicides. The relevant Si 2*p* line full width at half maximum (FWHM) is reduced and in any case the centroid of the line is shifted back towards higher binding energies, mainly because of the removal of the broad tail at low binding energies, as can be seen in Fig. 3. Even after annealing, the Si 2*p* line binding energy still depends on the initial composition, as shown in Fig. 2. For compositions close to FeSi₂, the Si 2*p* line shapes are quite identical but a slight change of the silicide composition induces a significant binding-energy decrease (see Table I). In any case, Figs. 1 and 2 clearly demonstrate that the spin-orbit-split doublet is less resolved for Si-rich silicides than for Fe-rich ones. For Si-rich silicides the Si 2*p* lines can no longer be assigned to a single Si environment.

Let us now comment on the Fe core-level-related lines shown in Fig. 4. The lower spectra are measured on ϵ -FeSi and β -FeSi₂. As opposed to the semiconducting β -FeSi₂-related Fe 2*p*_{3/2} line which is symmetric, the ϵ -FeSi-related core line exhibits a strong asymmetry. This effect has been observed previously on the Fe 3*p* lines measured on such compounds. As pointed out in Ref. 30, this asymmetry seems surprisingly large for ϵ -FeSi, which is a narrow-gap semiconductor. However, such a large asymmetry could originate from the strong correlation within the narrow *d* band expected in ϵ -FeSi, possibly responsible for its unusual magnetic properties.³⁸ Indeed a localized character of the *d* electrons usually results in satellite or shake-up structure in the core-level photoemission spectra. Furthermore, ϵ -FeSi is not a typical semiconductor. Its energy gap (0.05 eV) is very small and the narrow forbidden region is surrounded on both the

valence and conduction band side by a rapidly increasing density of states with strong 3*d* character.³⁹ Thus various kinds of low-energy excitations (compared to the experimental resolution), such as electron-hole pair or atomic multiplets, may become important and could explain the very strong core-line asymmetry observed for ϵ -FeSi. Additionally, this suggests that core holes created in the photoemission process are better screened, at room temperature, in ϵ -FeSi than in β -FeSi₂. This could explain the shift of both Si 2*p* and Fe 2*p*_{3/2} lines towards lower binding energies with respect to that in β -FeSi₂.

The metastable silicides related Fe 2*p*_{3/2} lines binding energy are just between those of β -FeSi₂ and ϵ -FeSi and show only a negligible dependence on the composition. After RT deposition (not shown), the Fe 2*p*_{3/2} line binding energy is lower than that of β -FeSi₂ by about 0.20 eV for the Fe-rich silicides (FeSi, FeSi_{1.3}, FeSi_{1.5}) and by about 0.30 eV for compositions close to FeSi₂. These lines are also asymmetric, but in this case the asymmetry is consistent with the fact that all metastable silicides are metallic.^{2,25} After annealing these layers just below the metastable-to-stable transition temperature, Fe 2*p*_{3/2} lines have the same binding energy over the whole FeSi to FeSi₂ composition. It is shifted by 0.20 eV with respect to β -FeSi₂ towards lower binding energies. Note that the Fe 2*p*_{3/2} line shape and FWHM are the same for unannealed or annealed pseudomorphic silicides.

IV. DISCUSSION

All spectroscopic data (presented in this work or published elsewhere) indicate that metastable Fe silicides have definitely different electronic characteristics than the bulk stable β -FeSi₂ and ϵ -FeSi silicides. Core-level binding energies are very close together for all metastable Fe silicides investigated in this work. This has to be related to similar silicide crystallographic structures, over a wide composition range (from FeSi to about FeSi_{1.8}). As a matter of fact FeSi crystal has a CsCl-type symmetry which seems to be preserved upon increasing the Si content in these codeposited silicides, as it was shown by XRD, reflection high-energy electron diffraction, and x-ray photoelectron diffraction measurements.^{7,14} To explain the persistence of this symmetry and in order to preserve the silicide stoichiometry, von Känel *et al.*⁷ proposed a structural model for the FeSi_{*x*} (1 < *x* < 2) phases. FeSi₂ could be derived from FeSi by forming randomly distributed Fe vacancies in the CsCl-type lattice. Another disilicide structure has been recently proposed on the basis of grazing-incidence x-ray-diffraction (GXR) experiments. Jedrecy *et al.*¹² have shown that MOCVD as well as thin SPE-grown FeSi₂ silicides crystallize in a tetragonal α -FeSi₂ derived structure. GXR measurements indicate that 15–20 % of the Fe atoms must be shifted from their positions in perfect α -FeSi₂ lattice and randomly distributed over unoccupied octahedral sites. Both CsCl and α -FeSi₂-derived structures have lattice parameters very close together and exhibit similar local atomic order around Fe and Si atoms. This is why

EXAFS measured on codeposited FeSi₂, at the Fe *K* edge (Ref. 14) is consistent with both structures as far as the Fe coordination shells are concerned. From EXAFS data, Fe atoms are surrounded by Fe-Si nearest neighbor (NN) and Fe-Fe next-nearest-neighbor (NNN) shells at distances less than 3 Å. The bond lengths and coordination numbers were found to depend on the stoichiometry. They are summarized in Table II. The first coordination shell of Fe atoms is only slightly dependent on the stoichiometry since in all pseudomorphic silicides, Fe atoms are bonded to eight Si NN at distances of about 2.35–2.37 Å. The second coordination shell was found to be very sensitive to the silicide composition. Indeed, Fe-Fe NNN bond lengths are of 2.75 Å in FeSi and 2.69 Å in FeSi₂ and the relevant coordination numbers decrease from 6 for FeSi down to about 3 or 4 for FeSi₂. The reduction of the NNN coordination numbers results in a substantial decrease of the lattice parameter. It is of 2.77 Å for FeSi and 2.70 Å for FeSi₂.² Furthermore, EXAFS analysis indicate a deviation from a perfect cubic lattice for both room-temperature deposited or annealed FeSi₂ compounds. Assuming a CsCl-type FeSi derived structure for all silicides, one would expect a different behavior for the Fe and Si core-electron states binding energies versus composition, related to changes in NN environment. Indeed, upon changing the stoichiometry from FeSi to FeSi₂, NN environment of Fe atoms does not change. In any case Fe atoms are surrounded by eight NN Si atoms (see Fig. 5). Thus Fe 2*p*_{3/2} lines are expected to be rather insensitive to the formation of Fe vacancies, as it is experimentally observed on annealed silicide, since the formation of Fe vacancies in a CsCl lattice would mainly affect the second coordination shell. The influence of the next-nearest neighbors can be assumed to be quite small since the electronic structure of transition-metal silicides is generally well described by the tight-binding approximation and largely determined by local atomic order.

For the Si-related core levels the situation is somewhat different. As opposed to the Fe atom environment, the Si atoms first coordination shell is highly composition dependent within these models. It is composed of eight NN Fe atoms in FeSi and a mean value of four NN Fe atoms in both proposed FeSi₂ structures. As shown pre-

viously, the Si 2*p* line shape is consistent with Si atoms located in a single Si site, at a FeSi composition. A possible origin of the Si 2*p*-related binding-energy shift with respect to β-FeSi₂ or clean Si(111) can be found in a recent theoretical work of Mäder, von Känel, and Baldereschi.⁴⁰ Their calculations show that a small electronic charge (0.18 electron per Si atom) is transferred from silicon to iron in the CsCl-type FeSi structure. The relevant Si 2*p* core-line shift towards higher binding energies observed in these experiments might be understood by the partially ionic binding character. From Si 2*p* core-level shifts observed in Si—F, Si—O, and Si—Cl bonds⁴¹ with respect to Si (111), Si 2*p* binding-energy shifts can be estimated to about 2 eV core-level shift per unit charge. A 0.18 electron charge transfer from silicon to iron would induce a Si 2*p* binding-energy shift of about 0.36 eV towards higher binding energies. This value has the sign and the order of magnitude of that measured in Figs. 1 and 2. The FeSi-related Si 2*p* line binding-energy shift is referred to the β-FeSi₂-related Si 2*p* line binding energy. The β-FeSi₂ phase crystallizes in an orthorhombic structure which can be thought of as a distortion of a CaF₂-type structure. Calculations performed by Mäder, von Känel, and Baldereschi show that ionicity is negligible in the CaF₂-type FeSi₂ structure and that the bonding configuration of CaF₂-type FeSi₂ is very similar to that of CoSi₂ and NiSi₂. Since β-FeSi₂ differs from the CaF₂ structure only through small deformations of the cubic cages in the fluorite structure,³⁶ the nonionic character of the Fe—Si bonds could be preserved and β-FeSi₂ could be used as a reference for the Si 2*p* line shift.

On the other hand, at a strict FeSi₂ stoichiometry the mean Fe NN coordination number $\langle N_{\text{Fe}} \rangle$ would be 4 (instead of 8 in FeSi) and is the most probable environment around a given Si atom. Introducing iron vacancies in the CsCl lattice reduces the NN coordination number around a given Si atom and thus the possibility of electron transfer from Si to Fe. A reduction of the Si 2*p* shift is expected when the Si content is increased in the silicide. Additionally, due to a statistical distribution of Fe vacancies over the silicide structure proposed in models of Ref. 7, Si sites with a Fe NN coordination number lower and higher than the $\langle N_{\text{Fe}} \rangle$ value have to be taken into account. The Si 2*p* lines would be composed of

TABLE II. Structural parameters deduced from the analysis of EXAFS spectra recorded at the Fe *K* edge from iron silicides epitaxially grown on Si(111) (from Ref. 14). *R* and *N* are the bond lengths and coordination numbers, respectively. The Debye-Waller factor difference $\Delta\sigma$ is related to Fe—Si and Fe—Si bonds in a high-temperature-annealed thin (30 Å) FeSi₂ film.

Compounds	Pair	<i>R</i> (Å)	<i>N</i>	$\Delta\sigma$ (Å)
FeSi ₂ (30 Å) (annealed at 600 °C)	Fe-Si	2.35±0.02	8±0.5	0
	Fe-Fe	2.68±0.02	3±0.5	0
FeSi _x (<i>x</i> ≈ 2) (90 Å) (RT deposited)	Fe-Si	2.34±0.02	8±0.5	0.04
	Fe-Fe	2.69±0.02	3.4±0.05	0.03
FeSi (90 Å) (RT deposited)	Fe-Si	2.37±0.02	8±0.5	0.06
	Fe-Fe	2.75±0.02	6.0±0.5	0.06

several chemically shifted components, as it is indeed observed experimentally. Si sites with low Fe NN coordination numbers would contribute to Si 2*p* lines shifted towards lower binding energies, as compared to FeSi. Such a statistical distribution of Si sites is evidenced on all FeSi_{*x*} (with *x* > 1) experimental Si 2*p* spectra by Si 2*p* components at binding-energy values close to that of β-FeSi₂ or clean Si(111). Spectra of Figs. 1–3 show that the low binding-energy components increase with Si content giving rise to a broad unresolved Si 2*p* line for FeSi_{1.8} or FeSi₂ compositions. The low binding-energy Si 2*p* contribution is larger for Si-rich silicide than for Fe-rich silicides, in agreement with a structural model, in which the FeSi_{*x*} silicide structure is deduced from a true CsCl-type FeSi phase by introducing iron vacancies.

Note that for the Si-rich silicides (~ FeSi₂), the large Si site distribution affects not only the Si 2*p* linewidth but also the silicide morphology and structure. Lattice distortions induced by these numerous possible sites are evidenced by LEED and EXAFS measurements.¹⁴ Indeed, the LEED pattern quality is strongly degraded upon a slight increase of the Si content within the silicide film, for compositions close to FeSi₂. Furthermore, EXAFS data indicate a deviation from a perfect cubic crystal for RT codeposited disilicides. Upon annealing, the Si 2*p* lines are shifted back towards higher binding energies and the spin-orbit-splitted doublet resolution is improved. This is not observed for Fe-rich silicides. Indeed, Figs. 1–3 show that the shape of the Si 2*p* line measured on FeSi, FeSi_{1.3}, and FeSi_{1.5} does not change significantly upon annealing. The reduction of the Si 2*p* line FWHM upon annealing RT-deposited FeSi₂ layers suggests that the vacancy distribution over annealed Si-rich silicide is probably not as random as one could expect. EXAFS measurements on both RT-deposited and annealed thin (600 °C) and thick (400 °C) FeSi₂ layers indicate that the cubic structure is no longer preserved for these compositions. It seems that, when starting from a poorly ordered

FeSi_{*x*} (*x* ~ 2) silicide, as is the case for RT codeposited ones, the silicide adopts a structure which deviates from a cubic one. This structure could be close to the α-FeSi₂ derived phase proposed in Ref. 12. Si 2*p* core lines of the stable α-FeSi₂ phase have been measured by Sirotti *et al.*³⁰ It was found to be shifted by about 0.20 eV towards higher binding energies, with respect to the Si(111) 7×7 one.

However, Si 2*p* and Fe 2*p*_{3/2} binding energies as well as line-shape evolution versus composition over a wide composition range, from FeSi to about FeSi_{1.8}, could be explained assuming a nearly cubic CsCl-type structure in which Fe vacancies are randomly distributed over the Si cages. This conclusion is fully consistent with EXAFS measurements¹⁴ which indicate that the cubic CsCl-type metastable silicide structure is preserved when passing at least from FeSi to FeSi_{1.5}.

V. CONCLUSIONS

Si 2*p* and Fe 2*p*_{3/2} core-electron states have been measured on codeposited pseudomorphic FeSi_{*x*} (1 < *x* < 2) silicides using monochromatized x-ray photoemission. The core-level line shapes as well as binding energies have been compared to stable Fe silicide ones. It was shown that metastable epitaxial FeSi_{*x*} have definitively different spectroscopic signatures than stable phases. Substantial Si 2*p* binding-energy shifts, with respect to stable β-FeSi₂, may be interpreted in terms of charge transfer from Si to Fe, according to recent theoretical calculations. Si 2*p* and Fe 2*p*_{3/2} binding-energy variations versus composition are consistent with those expected for FeSi_{*x*} layers with the structure proposed in the literature. Furthermore, the spectroscopic data collected on these pseudomorphic phases must be taken into account for a complete description of Fe silicides formed at the Fe/Si(111) interface.

*Present address: Laboratorium für Festkörperphysik, Eidgenössische Technische Hochschule Zürich, 8093 Zürich, Switzerland.

¹M. C. Bost and J. E. Mahan, *J. Appl. Phys.* **64**, 2034 (1988); C. Giannini, S. Lagomarsino, F. Scarinci, and P. Castrucci, *Phys. Rev. B* **45**, 8829 (1992).

²N. Onda, H. Sirringhaus, S. Goncalves-Conto, C. Schwartz, E. Müller-Gubler, and H. von Känel, in *Evolution of Surface and Thin Film Microstructure*, edited by H. A. Atwater, E. Chason, M. Grabow, and M. Lagally, MRS Symposia Proceedings No. 280 (Materials Research Society, Pittsburgh, 1993), p. 581.

³M. G. Grimaldi, P. Baeri, C. Spinella, and S. Lagomarsino, *Appl. Phys. Lett.* **60**, 1132 (1992).

⁴H. von Känel, R. Stalder, H. Sirringhaus, N. Onda, and J. Henz, *Appl. Surf. Sci.* **43**, 196 (1991).

⁵A. L. Vazquez de Parga, J. De la Figuera, C. Ocal, and R. Miranda, *Europhys. Lett.* **18**, 595 (1992).

⁶N. Onda, J. Henz, E. Müller, K. A. Mäder, and H. von Känel,

Appl. Surf. Sci. **56-58**, 421 (1992).

⁷H. von Känel, K. A. Mäder, E. Müller, N. Onda, and H. Sirringhaus, *Phys. Rev. B* **45**, 13 807 (1992).

⁸U. Kafader, P. Wetzel, C. Pirri, and G. Gewinner, *Appl. Surf. Sci.* **70/71**, 573 (1993).

⁹U. Kafader, M. H. Tuilier, C. Pirri, P. Wetzel, G. Gewinner, D. Bolmont, O. Heckmann, D. Chandéris, and H. Magnan, *Europhys. Lett.* **22**, 529 (1993).

¹⁰J. Chevrier, P. Stocker, V. Le Thanh, J. M. Gay, and J. Derrien, *Europhys. Lett.* **22**, 449 (1993).

¹¹N. Jedrecy, Y. Zheng, A. Waldhauer, M. Sauvage-Simkin, and R. Pinchaux, *Phys. Rev. B* **48**, 8801 (1993).

¹²N. Jedrecy, A. Waldhauer, M. Sauvage-Simkin, R. Pinchaux, and Y. Zheng, *Phys. Rev. B* **49**, 4725 (1994).

¹³X. W. Lin, M. Behar, J. Desimoni, H. Bernas, J. Washburn, and Z. Liliental-Weber, *Appl. Phys. Lett.* **63**, 105 (1993).

¹⁴C. Pirri, M. H. Tuilier, P. Wetzel, S. Hong, D. Bolmont, G. Gewinner, R. Cortès, and O. Heckmann, *Phys. Rev. B* **51**, 2302 (1995).

- ¹⁵A. Kakisaki, H. Suguwara, I. Nagakura, Y. Ischikawa, Komatsubara, and T. Ischii, *J. Phys. Soc. Jpn.* **51**, 2597 (1982).
- ¹⁶G. Shirane, J. E. Fischer, Y. Endoh, and K. Tajima, *Phys. Rev. Lett.* **59**, 351 (1987).
- ¹⁷B. Egert and G. Panzner, *Phys. Rev. B* **29**, 2091 (1984).
- ¹⁸N. E. Christensen, *Phys. Rev. B* **42**, 7148 (1990).
- ¹⁹M. De Crescenzi, G. Gaggiotti, N. Motta, F. Patella, A. Balzarotti, and J. Derrien, *Phys. Rev. B* **42**, 5871 (1990).
- ²⁰S. J. Oh, J. W. Allen, and J. M. Lawrence, *Phys. Rev. B* **35**, 2267 (1987).
- ²¹A. Rizzi, H. Moritz, and H. Lüth, *J. Vac. Sci. Technol. A* **9**, 912 (1991).
- ²²K. Lefki, P. Muret, E. Bustarret, N. Boutarek, R. Madar, J. Chevrier, J. Derrien, and M. Brunel, *Solid State Commun.* **80**, 791 (1991).
- ²³X. Wallart, H. S. Zeng, J. P. Nys, and G. Dalmai, *Appl. Surf. Sci.* **56-58**, 427 (1992).
- ²⁴U. Kafader, C. Pirri, P. Wetzel, and G. Gewinner, *Appl. Surf. Sci.* **64**, 297 (1993).
- ²⁵U. Kafader, P. Wetzel, C. Pirri, and G. Gewinner, *Appl. Phys. Lett.* **63**, 2360 (1993).
- ²⁶U. Kafader, P. Wetzel, C. Pirri, and G. Gewinner, *Appl. Surf. Sci.* **70/71**, 573 (1993).
- ²⁷J. Alvarez, A. L. Vazquez de Parga, J. J. Hinarejos, J. De la Figuera, E. G. Michel, C. Ocal, and R. Miranda, *J. Vac. Sci. Technol. A* **11**, 929 (1993).
- ²⁸J. Alvarez, A. L. Vazquez de Parga, J. J. Hinarejos, J. De la Figuera, E. G. Michel, C. Ocal, and R. Miranda, *Phys. Rev. B* **47**, 16048 (1993).
- ²⁹M. Kasaya, S. Yamauchi, M. Hirai, M. Kusaka, M. Iwami, H. Nakamura, and H. Watabe, *Appl. Surf. Sci.* **75**, 110 (1994).
- ³⁰F. Sirotti, M. De Santis, X. Jin, and G. Rossi, *Phys. Rev. B* **48**, 8299 (1993).
- ³¹F. Sirotti, M. De Santis, X. Jin, and G. Rossi, *Phys. Rev. B* **49**, 11134 (1994).
- ³²S. A. Chambers, *Surf. Sci. Rep.* **16**, 261 (1992).
- ³³A. L. Vazquez de Parga, J. De la Figuera, C. Ocal, and R. Miranda, *Ultramicroscopy* **42-44**, 845 (1992).
- ³⁴J. Chevrier, V. Le Thanh, S. Nische, and J. Derrien, *Appl. Surf. Sci.* **56-58**, 438 (1992).
- ³⁵H. Sirringhaus, N. Onda, E. Müller-Gubler, P. Müller, R. Stalder, and H. von Känel, *Phys. Rev. B* **47**, 10567 (1993).
- ³⁶Y. Dusauroy, J. Protas, R. Wandji, and B. Roques, *Acta Crystallogr. Sec. B* **27**, 1209 (1971).
- ³⁷P. Villars and L. D. Calvert, *Pearson's Handbook of Crystallographic Data for Intermetallic Phases* (American Society for Metals, Metals Park, 1985).
- ³⁸K. R. A. Ziebeck, H. Capellmann, P. J. Brown, and P. J. Webster, *J. Magn. Magn. Mater.* **36**, 160 (1983).
- ³⁹L. Pauling and A. M. Soldate, *Acta Crystallogr.* **1**, 212 (1948).
- ⁴⁰K. Mäder, H. von Känel, and A. Baldereschi, *Phys. Rev. B* **48**, 4364 (1993).
- ⁴¹F. J. Himpsel, B. S. Meyerson, F. R. McFeely, F. J. Morar, A. Thaleb-Ibrahimi, and J. A. Yarmoff, in *Photoemission and Absorption Spectroscopy of Solids and Interfaces with Synchrotron Radiation*, Proceedings of the International School of Physics "Enrico Fermi," Course CVIII, edited by M. Campagna and R. Rosei (North-Holland, Amsterdam, 1990), p. 203, and references cited therein.